atmosphere

MDPI

Article

Atmospheric Dynamic Response to Coupling Currents to Wind Stress over the Gulf Stream

Jackie May [1,*] and Mark Bourassa [2]

[1] U.S. Naval Research Laboratory, Oceanography Division, Stennis Space Center, MS 39529, USA
[2] Center for Ocean-Atmospheric Prediction Studies (COAPS) & Department of Earth, Ocean and Atmospheric Science, Florida State University, Tallahassee, FL 32306, USA; mbourassa@coaps.fsu.edu
* Correspondence: jackie.may@nrlssc.navy.mil

Abstract: Atmospheric near-surface stress and boundary layer wind responses to surface currents are examined with high resolution coupled atmosphere–ocean models over the Gulf Stream during winter. Because the ocean and atmosphere are linked through surface stress, the two fluids can cause dramatic changes through feedback processes. When the current feedback is included, we find that the current gradient in the cross-wind direction drives the stress curl pattern and wind curl pattern to have minima and maxima at locations matching those of the ocean surface vorticity pattern. Furthermore, we find the large- (>30 km) and small-scale, or submesoscale (<30 km), stress curl and wind curl responses to ocean surface vorticity are complimentary; however, the large- and small-scale wind divergence responses are counteractive. These responses (commonly called coupling coefficients) are found to depend on the relative position to the Gulf Stream maximum current. Throughout the atmospheric boundary layer, we find including the current feedback also leads to changes in the atmospheric secondary circulation on either side of the Gulf Stream extension. The winter seasonal means suggest the current feedback will impact climate, and investigating individual events, such as an atmospheric front passing over the Gulf Stream, suggests the current feedback will also impact the intensity of weather.

Keywords: ocean currents; wind stress; current feedback; atmosphere and ocean coupled modeling; marine atmospheric boundary layer; secondary wind circulation; vorticity; submesoscale

Citation: May, J.; Bourassa, M. Atmospheric Dynamic Response to Coupling Currents to Wind Stress over the Gulf Stream. *Atmosphere* **2023**, *14*, 1216. https://doi.org/10.3390/atmos14081216

Academic Editors: Yubin Li and Jie Tang

Received: 3 July 2023
Revised: 20 July 2023
Accepted: 20 July 2023
Published: 28 July 2023

1. Introduction

High-resolution, coupled ocean–atmosphere models are sensitive to both the thermodynamic and dynamic sea state. Thermodynamically, the atmosphere responds to changes in the sea surface temperature (SST) and the ocean responds to air–sea heat fluxes [1–5]. The SST feedback and thermodynamic coupling between the ocean SST and the atmosphere generally acts to decrease the wind speed, and subsequently the wind stress, over cool water, and to increase it over warm water [5,6]. Many studies [6–8] have determined that the curl of the surface wind stress is linearly correlated with the crosswind component of the SST gradient, particularly over SST fronts.

Dynamically, the atmospheric surface winds respond to changes in the surface currents and the ocean is forced by wind stress, which is related to the vertical shear of horizontal motion [9]. As such, current feedback refers to the two-way coupling that includes changes to the atmospheric surface winds and stress, as well as changes to the surface currents. When the current feedback is included, the wind stress is calculated using surface-relative winds instead of absolute winds (winds relative to the fixed Earth). Current feedback acts to reduce the mean surface stress when ocean currents are moving in the same direction as the wind, and increase the mean surface stress when ocean currents are moving in the opposite direction as the wind; stress is a function of wind shear. Additionally, changes in surface stress lead to changes in winds, with a weaker surface stress allowing winds to

accelerate due to the changed boundary conditions having a larger impact [8]. Including current feedback in a fully coupled model can also lead to changes in stress curl, energy transfer between the atmosphere and the ocean, Ekman pumping, and the Gulf Stream path [3,6,8,10].

Recent modelling studies have been used to examine the interaction of currents and surface stress through feedbacks. For example, Ref. [11] used idealized mesoscale eddies to find that current-related modification of surface stress (as opposed to temperature influences) was primarily responsible for stress-induced vertical motion in the ocean, known as Ekman pumping, although they noted that western boundary currents with strong SST gradients are an exception. Refs. [10,12,13] found that surface currents of ocean eddies induce a curl of the stress in the opposite rotation from the current, qualitatively consistent with the expectations in [11]. They also confirmed that the feedbacks associated with SST gradients are very small compared to the feedbacks associated with current gradients for applications of eddy kinetic energy and vertical motion; however, SST gradient feedbacks are important for eddy propagation [14]. Ref. [12] provided the first demonstration that the atmosphere responds to current-induced changes in surface stress, finding that the rate of change of stress due to currents is reduced when the current feedback is included. This reduction is also dependent on how waves influence surface stress [8]. Similarly, wave–current interactions [15,16] are expected to influence not only surface currents, but will also likely impact surface stress.

The current feedback impact on the atmospheric dynamics has only begun to be studied within high-resolution, both spatially and temporally, coupled models that include both the thermodynamic and dynamic feedbacks. Non-fully coupled models, such as ocean-only models, are only capable of capturing part of the current feedback, although modified surface wind parameterizations could be utilized in ocean-only simulations [17]. Conversely, coupled models are dependent on the surface fluxes, and some parameterizations are known to be influenced by waves [8]. However, the sea state dependency of stress remains highly controversial, with very different dependencies suggested in recent studies [15,16]. For this study, we focus only on a model that is dependent on wind speed and boundary layer dynamic stability (i.e., not dependent on sea state).

As discussed above, previous studies have generally focused on the near-surface impacts due to the direct impact from the current feedback. Neglecting the current feedback could also contribute significantly to obtaining inaccurate and unrealistic model results above the atmospheric log layer. This study aims to provide further insight into the atmospheric dynamic response to the current feedback by focusing on two primary goals. First, we will provide further understanding of the separate current feedback impacts to the surface winds and stresses by separating the responses (i.e., coupling coefficients) into small-scale (<30 km) vs. large-scale (>30 km). Second, we will provide new insight into the dynamic response to the current feedback impacts throughout the atmospheric boundary layer. We also present new results related to the dynamic responses both at the surface and throughout the boundary layer based on the relative position of the maximum current within the Gulf Stream extension.

This paper is organized by describing the coupled modelling framework and the model experiments in Section 2. The small-scale vs. large-scale atmospheric surface wind and stress responses to the current feedback are presented in Section 3.1, along with the physical processes driving these responses. Atmospheric secondary circulations throughout the atmospheric boundary layer consisting of surface divergence and vertical motion that are produced in response to the current feedback are presented in Section 3.2. The discussion in Section 4 provides an overview and conceptual diagram of the primary and secondary impacts of the current feedback on the atmospheric dynamics on either side of the Gulf Stream extension, followed by the conclusions in Section 5.

2. Methods

2.1. Model Description

The regional high-resolution coupled modeling system used in this study was the Coupled Ocean–Atmosphere Mesoscale Prediction System (COAMPS), version 5.8. COAMPS consists of three modeling components: the Navy Coastal Ocean Model (NCOM), the COAMPS atmospheric model (COAMPS_ATM), and a wave model that the user can choose from. COAMPS allows for uncoupled, two-way, and three-way coupling between the ocean, atmospheric, and wave modeling components. The modeling components are integrated together through the Earth System Modeling Framework (ESMF) interface, as described by [18]. As discussed in the Introduction, we are not considering the sea state dependency on stress or currents in this study; therefore, the wave model was not included. For this study, only two-way coupling between the atmosphere and the ocean was considered, with the atmospheric and ocean model domains shown in Figure 1.

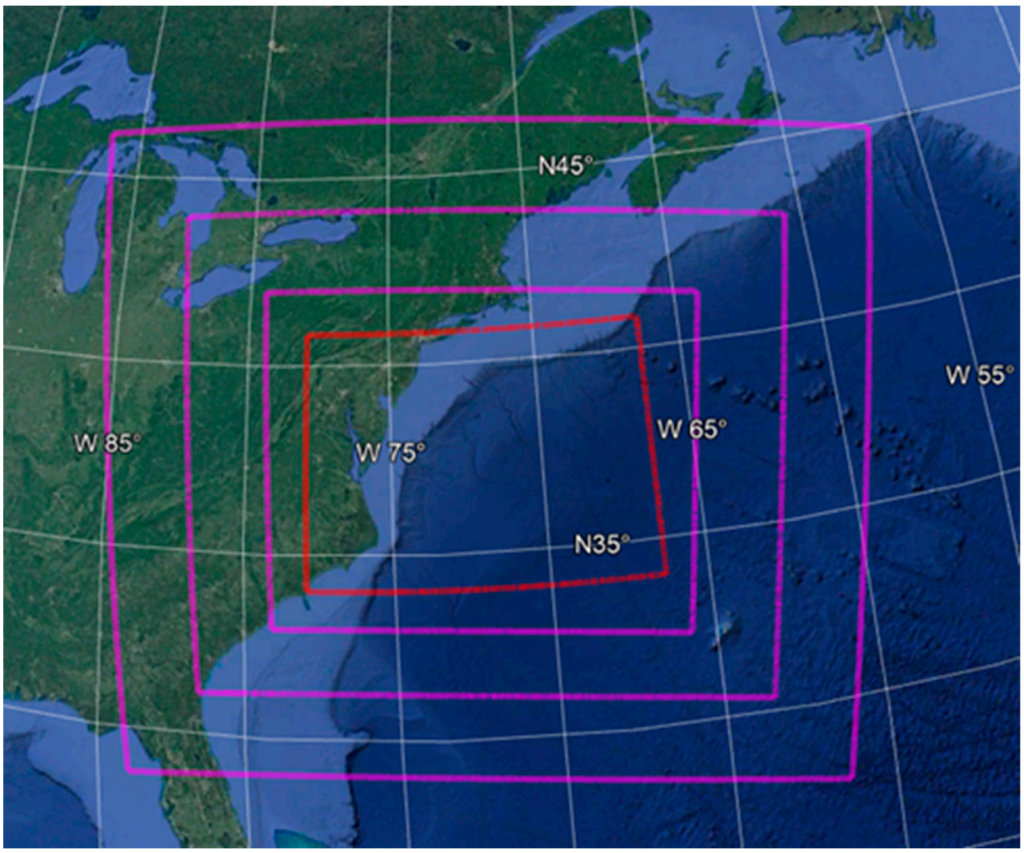

Figure 1. The three nested atmospheric domains (purple) and the single ocean domain (red) used in the COAMPS model simulations. The nested atmospheric domains have grid spacings of 18 km, 6 km, and 2 km. The ocean domain has a grid spacing of 0.02°.

2.1.1. COAMPS Atmospheric Model

The atmospheric model component was COAMPS_ATM version 5.4 [19]. The atmospheric simulations were performed on a Lambert conic conformal map projection centered on 37° N and 73° W consisting of 3 nests, with two-way nesting (Figure 1). The grid spacings of the nests were: 18 km (124 × 107 grid points), 6 km (287 × 233 grid points), and 2 km (615 × 487 grid points). Each atmospheric grid used 60 vertically-stretched levels. The outer nest used a 60 s time step, while the inner nests used a 3:1 time step ratio. The COAMPS_ATM configuration was set up with the following parameterizations: the Mellor and Yamada level 2.5 planetary boundary layer scheme [20]; the Fu–Liou radiation scheme [21,22] to calculate solar and longwave fluxes; and the Kain–Fritsch convective parameterization scheme [23,24] in the outer 18 km nest, while the inner nests had the

convective parameterization turned off (convection was explicit rather than parameterized). Atmospheric data assimilation was turned off. Initial and lateral boundary conditions for the outer 18 km nest were updated every 3 h from the 0.5° × 0.5° U.S. Navy Global Environmental Model (NAVGEM [25]).

2.1.2. NCOM Ocean Model

The ocean model component was NCOM version 4.5 [26]. The ocean simulations were performed on a spherical map projection within the 2 km atmospheric grid domain. A single 0.02° grid was used with 576 × 340 grid points. The ocean grid used a 30 s time step and had 50 vertical levels, including 35 sigma levels. The Mellor–Yamada Level 2.5 turbulent (boundary layer) scheme [20] was used to parameterize the vertical mixing, and the 3rd order upwind scheme was used for advection of tracers [27]. Similar to COAMPS_ATM, ocean data assimilation was turned off within this study. Initial and boundary conditions were updated every 3 h from the 1/12° U.S. Navy Global Ocean Forecast System (GOFS 3.1, [28]), which is comprised of the global Hybrid Coordinate Ocean Model (HYCOM) two-way coupled with the Community Ice CodE (CICE, [29]). The ocean model was forced with wind stress, precipitation, sea level pressure, and surface heat fluxes from the atmospheric model.

2.1.3. Coupling

In this model setup, ocean–atmosphere coupling was only active within the 2 km ocean domain. The 18 and 6 km atmospheric nests were run as atmospheric-only models (i.e., not coupled to NCOM); therefore, the ocean surface forcing fields were obtained from GOFS 3.1. The coupled ocean–atmosphere model simulations were run with a 6 min coupling interval between the atmosphere and ocean, and with hourly output fields. The surface momentum and turbulent heat fluxes were calculated within COAMPS_ATM using the SST field from NCOM and the COARE 2.5b formulation [30,31]. The vector wind stress ($\vec{\tau}$) is expressed as follows:

$$\vec{\tau} = \rho \vec{u_*} \left| \vec{u_*} \right| \tag{1}$$

where ρ is the air density and $\vec{u_*}$ is the friction velocity. Friction velocity depends on the turbulent state of the atmosphere [32], which is related to the roughness of the surface, wind speed, and boundary layer stability, and is defined as:

$$\vec{u_*} \left| \vec{u_*} \right| = \left(\frac{k}{ln(z/z_0) - \psi} \right)^2 \vec{U}(z) \left| \vec{U}(z) \right| = C_{D(z)} \vec{U}(z) \left| \vec{U}(z) \right| \tag{2}$$

where $\vec{U}(z)$ is the vector wind at height z (10 m), k is von Karman's constant, z_0 is the roughness length, ψ is the profile stability function, and C_D is the bulk transfer coefficient for momentum (drag coefficient) at height z. The vector stress within COAMPS_ATM is therefore determined as follows:

$$\vec{\tau} = \rho C_{D10} \left| \vec{U}_{10} \right| \vec{U}_{10} \tag{3}$$

where 10 represents z = 10 m. Hereafter the 10 will be excluded in C_{D10}.

The vector wind at 10 m can be defined in two different ways: the absolute wind ($\vec{U}_{10abs}$), which is relative to the fixed earth, or the surface-relative wind ($\vec{U}_{10rel}$), which is relative to surface currents ($\vec{U}_{curr}$). The relationship between the absolute and surface-relative winds is defined as $\vec{U}_{10rel} = \vec{U}_{10abs} - \vec{U}_{curr}$. As discussed in the Introduction, ocean surface currents can significantly modify the wind stress and curl of the surface stress through the current feedback. To investigate the current feedback impacts, the ocean surface currents were added as a feedback variable passed from NCOM to COAMPS_ATM,

which allows for the $\vec{U}_{10rel}$ term to be calculated within COAMPS_ATM. This feedback is in addition to the already existing SST feedback from NCOM to COAMPS_ATM. The vector stress for the simulations that include the current feedback is then determined as follows:

$$\vec{\tau} = \rho C_D \left| \vec{U}_{10abs} - \vec{U}_{curr} \right| \left(\vec{U}_{10abs} - \vec{U}_{curr} \right) = \rho C_D \left| \vec{U}_{10rel} \right| \vec{U}_{10rel} \quad (4)$$

2.2. Experiments

For this study, the model simulations were run from 1 November 2015–1 March 2016 over the Gulf Stream region, with hourly model outputs. Similar to the approach by [33], this includes a one-month model spin up during November, followed by a three-month analysis time period from December through February. Generally, a full season is sufficient for analysis to provide robust results and insight into the submesoscale impacts [34–36]. As we will show, the seasonal means presented here compare well with other studies that include multiple years. Additionally, having only one full season for analysis allows for more frequent model outputs, which are critical in determining physical processes associated with individual events. A winter time period was chosen because the upper ocean is much more turbulent with a large amount of submesoscale features during winter months [37,38]. This enhanced activity allows for the impact of the submesoscale features to be more easily explored. Two coupled atmosphere–ocean model experiments were performed with the only difference being in the definition of wind input in the surface stress calculation. The first simulation (a2o2) only included the SST feedback and computed the surface stress using $\vec{U}_{10abs}$, which is relative to the fixed earth. The second simulation (a2o2-cfb) included both the SST feedback as well as the current feedback and computed the surface stress using $\vec{U}_{10rel}$, which is relative to surface currents.

2.3. Spatial Filtering

To examine the separate impacts between the small-scale (submesoscale) and large-scale processes, a high-pass Gaussian spatial filter was applied to the model output fields. Different cutoff values, or smoothing lengths, have been used in previous studies to examine the ocean submesoscale impacts, ranging from 12.5 km [35] to 30 km [39] to 50 km [38,40]. For this study, a 30 km cutoff value was selected. For a given field (x), the large-scale field is defined as the spatially smoothed field after applying the Gaussian filter with a standard deviation of 30 km ($|x|$), and the small-scale field is the residual $x' = x - |x|$.

3. Results

3.1. Atmospheric Surface Impacts

The winter-time seasonal means of the ocean surface currents and vector surface stress over the Gulf Stream region are shown in Figure 2. Over the Gulf Stream extension, when the current feedback is included, there is a slight reduction in the current and stress magnitude due to the winds having a positive vector component aligned with the currents. Conversely, over the Gulf Stream path closer to the coastline, when the current feedback is included, there is a slight increase in the current and stress magnitude due to the winds having a negative vector component aligned with the currents. As expected, including the current feedback leads to an overall slight reduction in the winter-time seasonal mean of the current velocity (0.01 m s^{-1}), as well as in the stress magnitude (0.005 N m^{-2}) over the Gulf Stream region.

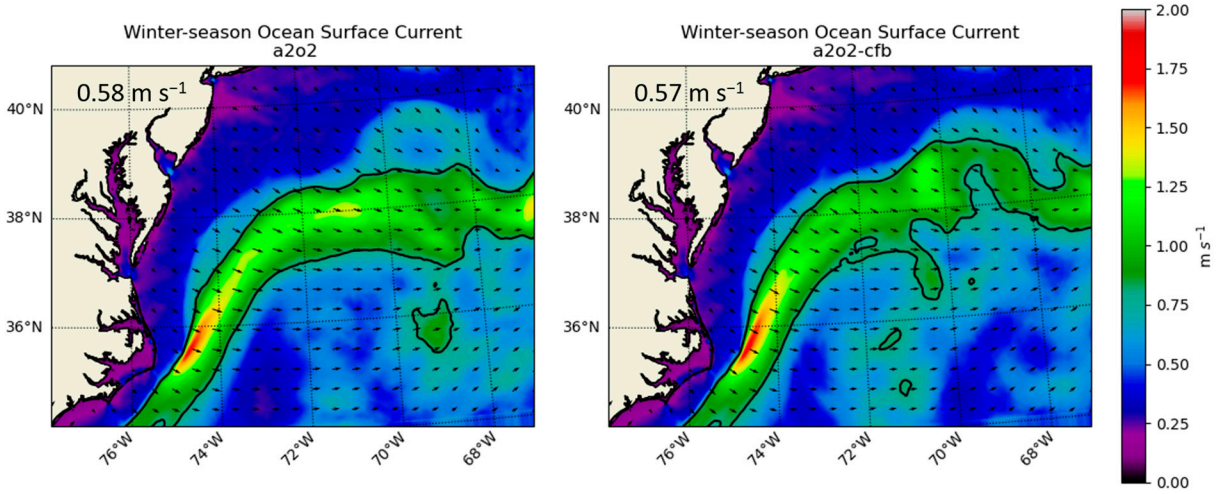

Figure 2. Winter-time seasonal mean of surface currents (shading) and vector winds (arrows) for the a2o2 (**left**) and a2o2-cfb (**right**) model simulations over the Gulf Stream region. The current velocity at 0.8 m s^{-1} is contoured and the seasonal mean surface current magnitude is shown in the top left of the panels.

To further explore the winter-time seasonal mean differences in the two simulations, PDFs of the primary surface parameters related to the current feedback are shown in Figure 3. The general trends in the PDFs for the two simulations are similar; however, there are key differences at the more extreme values. When the current feedback is included (orange lines) there is a narrower distribution at the more extreme surface current and wind stress magnitudes, and a wider distribution at the more extreme wind speed magnitudes. These results, in agreement with previous studies (i.e., [12]), imply the current feedback leads to a reduction in the mean current and stress magnitude, and an increase in the mean wind speed magnitude.

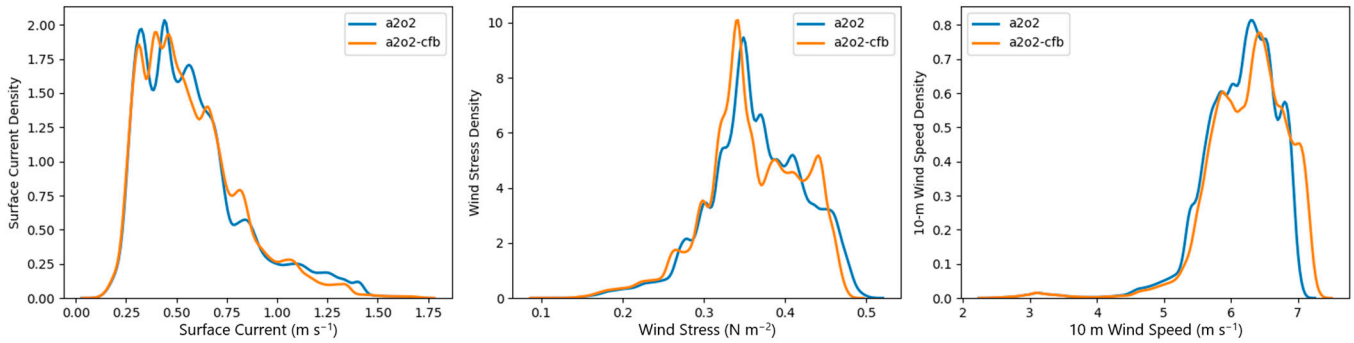

Figure 3. PDF of the winter-time seasonal mean surface current (**left**), wind stress (**middle**), and 10 m wind speed magnitude (**right**) for the a2o2 (blue line) and the a2o2-cfb (orange line) simulations.

Along with the changes in the surface current, stress, and wind fields, the inclusion of the current feedback also modifies the stress curl and wind curl based on the ocean surface vorticity (i.e., surface current curl). Corresponding to Figure 2, the winter-time seasonal mean of the surface current curl, wind stress curl, 10 m wind curl, and 10 m wind divergence over the Gulf Stream region are shown in Figure 4. Regardless of the inclusion of the current feedback, to the right of the maximum Gulf Stream extension current there is a large region of negative ocean-relative vorticity, and to the left of the maximum Gulf Stream extension current there is a slightly smaller region of positive ocean-relative vorticity.

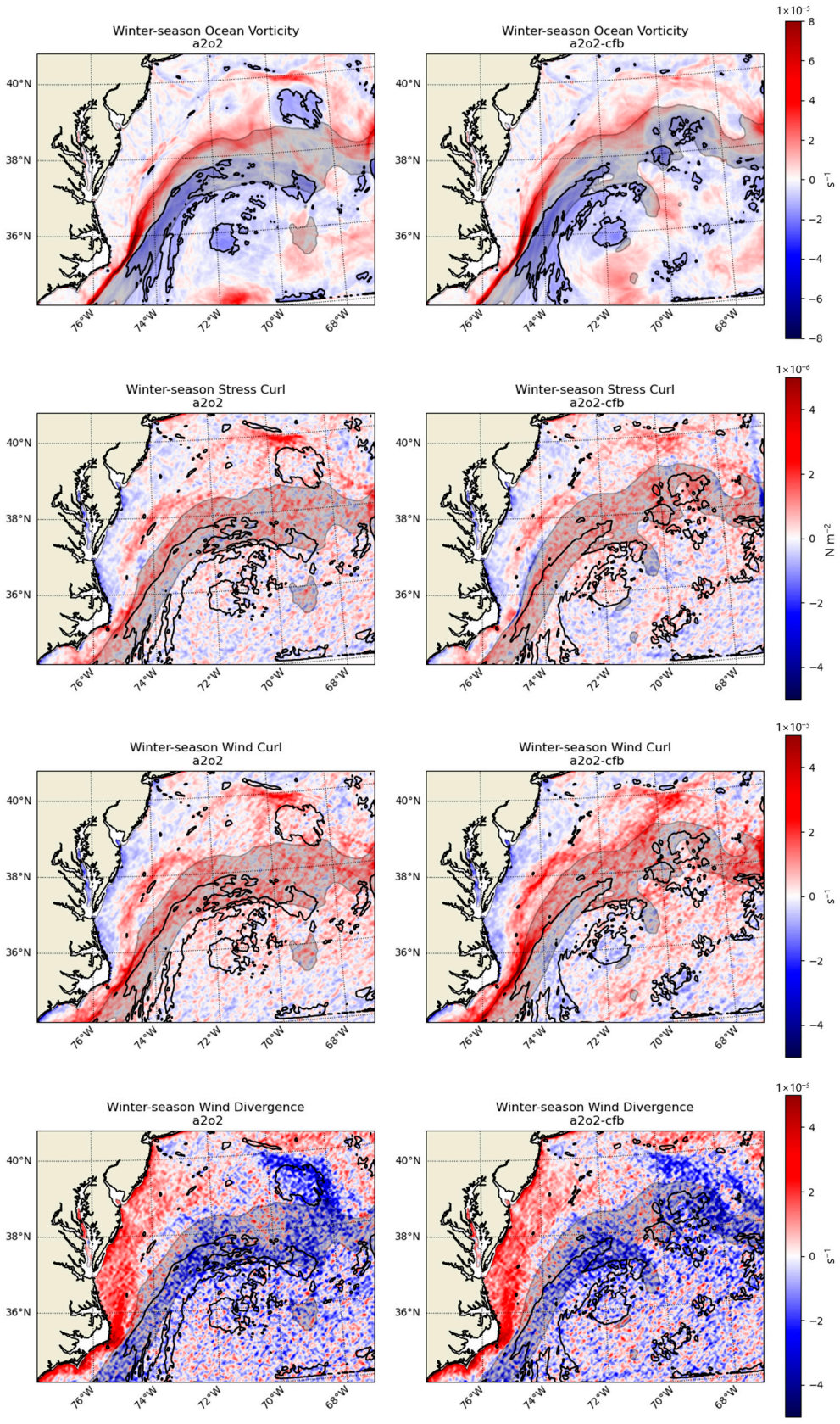

Figure 4. Winter-time seasonal mean of ocean-surface-relative vorticity (**top row**), stress curl (**2nd row**), 10 m wind curl (**3rd row**), and 10 m wind divergence (**bottom row**) for the a2o2 (**left**) and a2o2-cfb (**right**) simulations over the Gulf Stream region. The ocean surface vorticity at -8×10^{-6} m s^{-1} is contoured and the ocean surface current velocity greater than 0.8 m s^{-1} is shaded in grey.

Similar to the pattern observed with the ocean-relative vorticity, the surface wind divergence pattern also exists regardless of the inclusion of the current feedback, indicating a thermodynamic dependence. The surface wind divergence has been found to have a close relationship with the downwind SST gradient [6,7]. In the Gulf Stream extension region, the surface wind typically is from the west to northwest, which leads to generally positive divergence over the cooler water to the north of and overlapping with the Gulf Stream extension and negative divergence, or convergence, over the warmer water to the south of and overlapping with the Gulf Stream extension [41,42]. Due to the SST feedback dominating for the prevalent wind directions, negative ocean vorticity (generally right of the Gulf Stream extension) is typically associated with surface convergence, while positive ocean vorticity (generally left of the Gulf Stream extension) is associated with areas of surface divergence as well as areas of surface convergence.

The stress curl and wind curl patterns with respect to the ocean-relative vorticity pattern are found to be dependent on the current feedback [12]. When the current feedback is not included (a2o2), there is a slight positive relationship between the stress curl pattern and the ocean-relative vorticity, due to the SST feedback [1]. As discussed in the Introduction, the wind stress curl is proportional to the crosswind SST gradient; hence this SST-related response is a sinusoidal function of the wind direction relative to the SST gradient [43]. In contrast, current-induced wind curl is only weakly dependent on wind direction relative to the current gradient [43]. When current feedback is included (a2o2-cfb), it counteracts the SST feedback and allows for positive current vorticity to create a negative surface stress curl and a positive wind curl [12] in areas SST feedback would cause a negative wind curl, as seen in Figure 4. A positive ocean vorticity (generally left of the Gulf Stream extension) is found to be associated with negative stress curl and positive wind curl, while a negative ocean vorticity (generally right of the Gulf Stream extension) is found to be associated with positive stress curl and negative wind curl.

Figure 5 shows the corresponding PDFs of the winter-season parameter means shown in Figure 4. To more clearly identify differences between the models, the PDFs have been separated based on the corresponding ocean vorticity value. In agreement with the results above, the ocean vorticity and the wind divergence PDFs are very similar regardless of the inclusion of the current feedback. For negative ocean vorticity, current coupling causes the wind divergence PDF (solid lines) peak to be shifted to greater convergence, while the wind divergence peaks in regions of positive ocean vorticity (dashed lines) are shown to be close to zero. Conversely, the stress curl and wind curl patterns do show greater differences based on the current feedback. The a2o2 stress curl and wind curl peaks are shown to be close to zero. In regions of negative ocean vorticity, the a2o2-cfb stress curl peak is shifted towards positive values and the wind curl peak is shifted towards negative values. In regions of positive ocean vorticity, the a2o2-cfb stress curl peak is shifted towards negative values and the wind curl peak is shifted towards positive values. These results reinforce the relationships between ocean vorticity and stress curl, wind curl, and wind divergence discussed above.

3.1.1. Surface Stress Curl

Coupling coefficients have been used often in previous studies to show the linear relationship between two variables [6,12,33,44]. The surface stress response to including vs. neglecting the current feedback is determined with coupling coefficients between ocean surface current-relative vorticity and stress curl (s_τ). Separate coupling coefficients are calculated for positive vs. negative ocean-relative vorticity values. The hourly output fields were first temporally averaged using a 1-day running mean. Then, a 30 km high-pass Gaussian spatial filter was applied to separate the small-scale (submesoscale) impact vs. the large-scale impact.

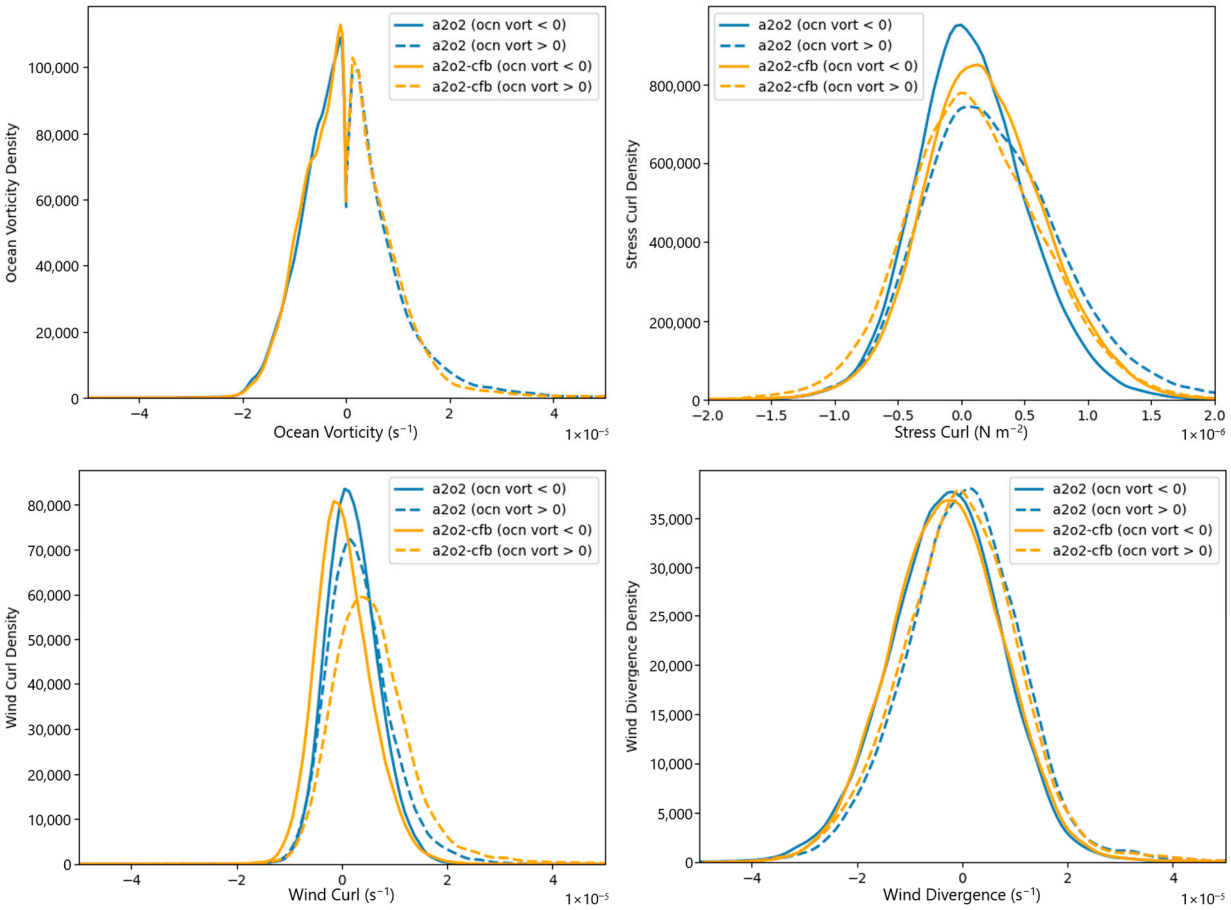

Figure 5. PDFs of the winter-time seasonal mean surface current vorticity (**top left**), wind stress curl (**top right**), 10 m wind curl (**bottom left**), and 10 m wind divergence (**bottom right**) for the a2o2 (blue lines) and the a2o2-cfb (orange lines) simulations. The solid lines correspond to negative ocean vorticity and the dashed lines correspond to positive ocean vorticity.

Binned scatterplots of the small-scale and large-scale s_τ over the winter season are shown in Figure 6. When the current feedback is not included (a2o2), there is generally a slight positive relationship between the ocean-relative vorticity and surface stress curl at both the small-scale and the large-scale. This is due to the SST feedback. When the current feedback is included (a2o2-cfb), there is a negative relationship between the ocean-relative vorticity and surface stress curl. This is expected from the discussion above and in agreement with previous studies. For example, Ref. [17] determined s_τ to be $\sim -2.9\ 10^{-3}$ N m^{-4} s^2 $|\,U_a\,|$ + 0.008 N m^{-3} s, based on a global coupled model simulation with a temporal average applied using a 29-day running mean and removing the large-scale signal with a 1° high-pass Gaussian spatial filter. If we assume an average wind speed of ~6.4 m s^{-1} (the 3-month average wind speed in our a2o2-cfb model simulation), then, following [17], s_τ should be ~ -0.0106 N m^{-3} s. This estimate is found to be similar to our a2o2-cfb average small-scale coupling coefficient ($s_\tau = -0.0163$ N m^{-3} s) and average large-scale coupling coefficient ($s_\tau = -0.0142$ N m^{-3} s). It is noted that there is a discontinuity in the linear relationship between negative and positive ocean vorticity values. This is likely a result of the thermal feedback partially counteracting the current feedback at low ocean vorticity and wind speeds, or impacts from other small-scale processes, such as atmospheric inertia gravity waves, near-inertial oscillations, and waves [45]. When a longer averaging window (i.e., 29 days) is applied to the hourly output, this discontinuity is dramatically reduced, which is expected if it is due to each of the processes mentioned above.

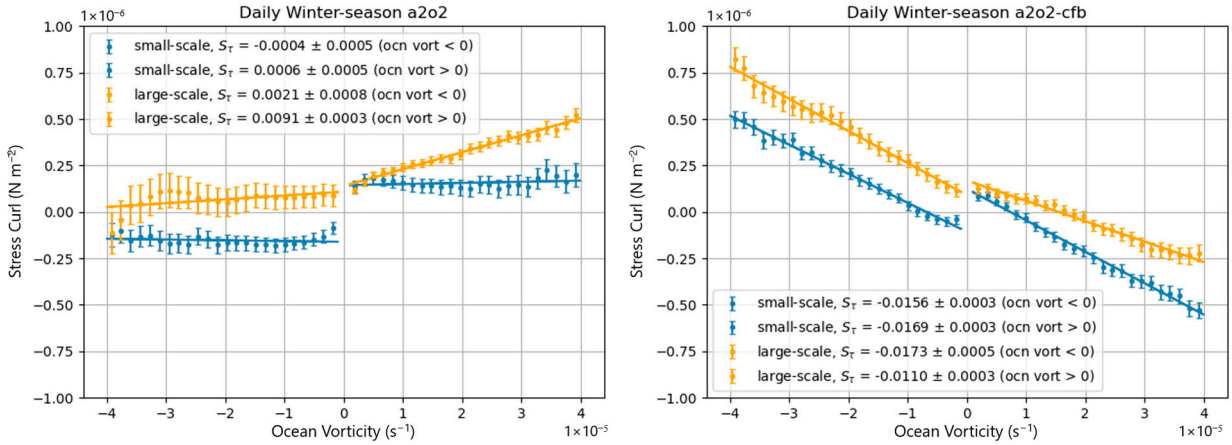

Figure 6. Binned scatterplot of the winter season time series of 1-day running mean of small-scale (<30 km, blue) and large-scale (>30 km, orange) wind stress curl and ocean-relative vorticity for the a2o2 (**left**) and the a2o2-cfb (**right**) simulations. Error bars represent the uncertainty in the mean with a 99.7% confidence [46]. The slope is the coupling coefficient in N s m^{-3}.

3.1.2. Ten Meter Wind Curl and Divergence

The 10 m wind response to including vs. neglecting the current feedback is shown with coupling coefficients between ocean surface current-relative vorticity and 10 m wind curl (s_w), as well as between ocean surface current-relative vorticity and 10 m wind divergence (s_d). Binned scatterplots of the small-scale and large-scale s_w and s_d over the winter season are shown in Figure 7. When the current feedback is not included (a2o2), the wind curl small-scale and large-scale coupling coefficient generally shows a slight positive relationship with the ocean-relative vorticity. When the current feedback is included (a2o2-cfb), the magnitude of both the small-scale and large-scale s_w increases dramatically and maintains the positive relationship. Our a2o2-cfb average small-scale coupling coefficient (s_w = 0.1917) and average large-scale coupling coefficient (s_w = 0.3505) agree well with previous studies. For example, Ref. [12] found s_w = 0.23 with a 150 km spatial filter applied over the California upwelling system and [43] found a mean value of s_w to be ~0.3 with a 1° spatial filter over the global oceans. s_w is noted to change regionally and seasonally because it is wind speed dependent.

While the current feedback leads to dramatic differences in the stress curl and wind curl patterns, there is less of an impact on the wind divergence. The authors of [17] discuss that the current feedback does not systematically impact the wind divergence because the oceanic currents are very nearly geostrophic and mainly rotational at the mesoscale. However, our model simulations have a 2 km ocean and atmosphere, which are submesoscale-permitting and are therefore impacted by submesoscale processes that do not necessarily follow geostrophy. Additionally, Ref. [33] determined that while the current feedback dominates the thermal (SST) feedback for the wind stress curl, it does have a smaller contribution for the wind stress divergence. The authors showed that including the current feedback leads to an increase in magnitude of the stress divergence coupling coefficient. Our results do show that when the current feedback is included, s_d generally increases in magnitude. For example, regardless of the inclusion of the current feedback, the small-scale wind divergence has a negative relationship with the ocean-relative vorticity. When the current feedback is included, our average small-scale coupling coefficient increases in magnitude from −0.01825 to −0.0409. The large-scale s_d is found to be dependent on the sign of the ocean-relative vorticity. Over positive ocean-relative vorticity, there is negative large-scale s_d that is complimentary to the small-scale s_d, and over negative ocean-relative vorticity, there is positive large-scale s_d that is counteractive to the small-scale s_d. When the current feedback is included, the large-scale s_d increases in magnitude from −0.0552 to −0.0979 over positive ocean-relative vorticity and decreases

in magnitude from 0.1857 to 0.1584 over negative ocean-relative vorticity. Additionally, we found the large-scale wind divergence is skewed towards negative divergence. This is due to the time-means being dominated by strong convergence associated with large storm systems [42]. These relationships imply that when the current feedback is included, the complimentary small-scale and large-scale motions lead to an enhancement of surface convergence over positive ocean-relative vorticity and the counteractive small-scale and large-scale motions lead to an enhancement of surface divergence over negative ocean-relative vorticity.

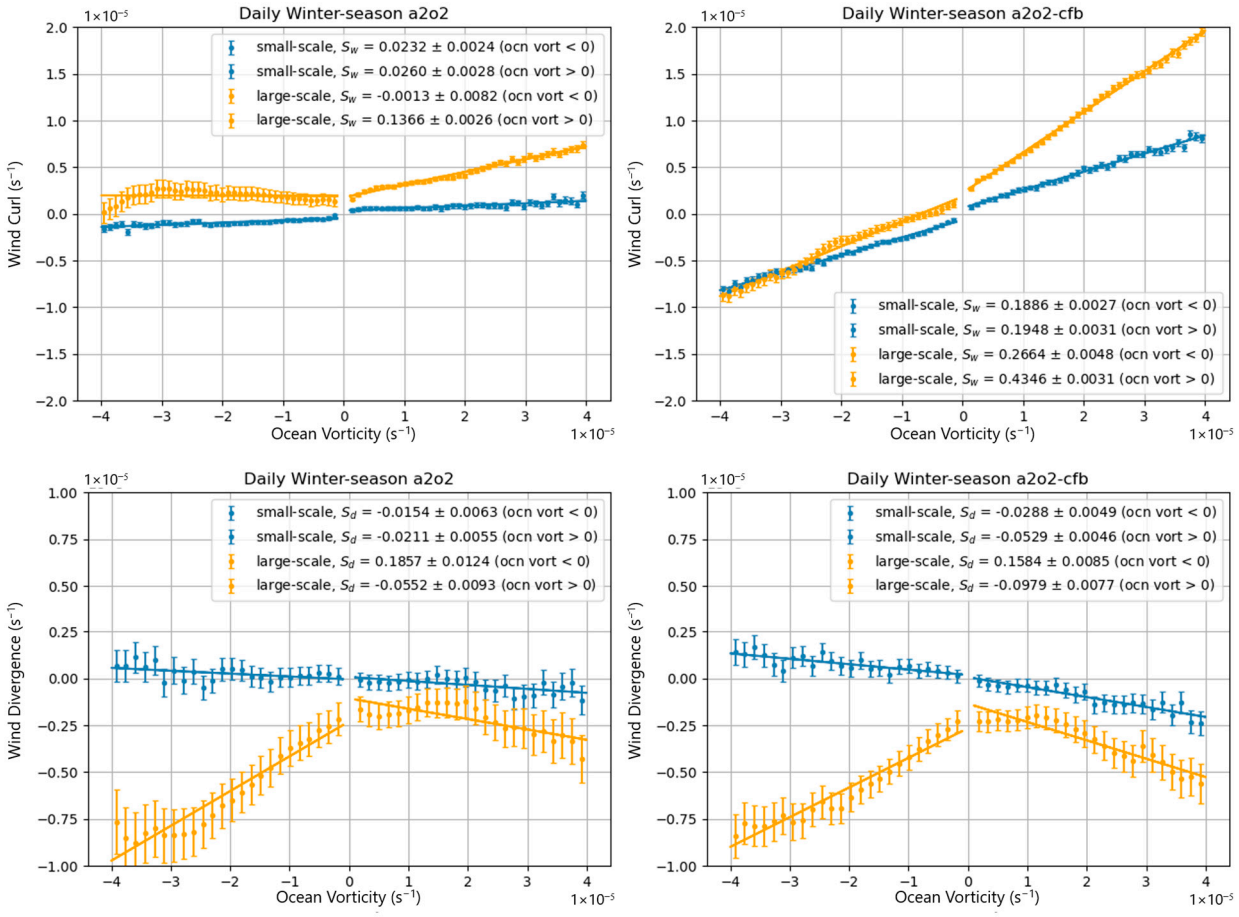

Figure 7. As in Figure 6, but for 10 m wind curl and ocean-relative vorticity (**top**) and 10 m wind divergence and ocean-relative vorticity (**bottom**). The slope is the coupling coefficient in dimensionless units.

3.1.3. Zonal Momentum Budget

Long-term averages, such as those shown and discussed above, provide statistically robust results and are used in determining broad dependencies; however, it is also necessary to examine individual time steps or events to identify physical processes involved. Because current feedback has its largest impacts when there is a large change in stress, areas associated with higher winds (i.e., atmospheric fronts) and stronger currents (i.e., the Gulf Stream) are ideal for investigating responses. Figure 8 shows a single snapshot example of an atmospheric front crossing the Gulf Stream extension on 1 January 2016 at 00 UTC. Here, we perform an analysis of the 10 m zonal momentum budget of this example to determine the primary physical processes associated with the surface wind variability.

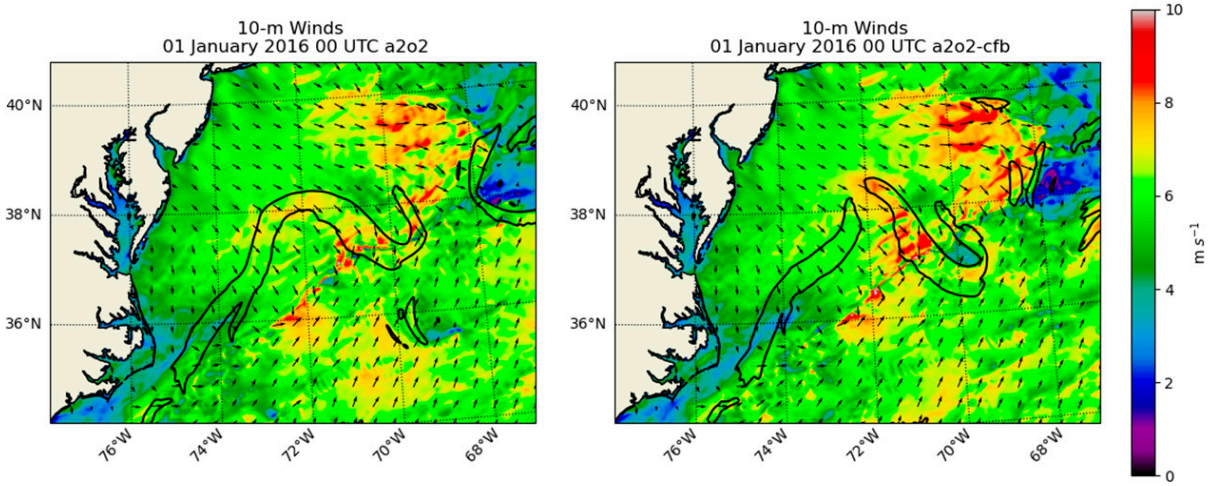

Figure 8. Surface wind field from 1 January 2016 at 00 UTC with an atmospheric front crossing the Gulf Stream extension, with surface current contoured at 1.2 m s^{-1} for the a2o2 (**left**) and the a2o2-cfb (**right**) simulations.

Following [2,19], the COAMPS_ATM zonal momentum budget is

$$\frac{\partial u}{\partial t} = -u\left(\frac{\partial u}{\partial x}\right) - v\left(\frac{\partial u}{\partial y}\right) - \dot{\sigma}\left(\frac{\partial u}{\partial \sigma}\right) + fv + D_u + K_H\nabla^4 u - C_p\theta_v\left(\frac{\partial \pi'}{\partial x} + \frac{\partial \sigma}{\partial x}\frac{\partial \pi'}{\partial \sigma}\right) \quad (5)$$

where u and v are the velocity components, σ is used for the transformation of the vertical coordinate, f is the Coriolis parameter, D_u represents the sub-grid scale vertical mixing, K_H is the horizontal mixing coefficient, C_p is the specific heat of air at constant pressure (1004 J kg^{-1} K^{-1}), and θ_v is the virtual potential temperature. π is related to pressure with the Exner function $\pi = (p/p_0)^{R_d/C_p} = \overline{\pi}(z) + \pi'(x, y, z, t)$, where p is pressure, p_0 is a reference pressure of 1000 hPa, and R_d is the dry gas constant (287 J kg^{-1} K^{-1}). The first three terms on the right-hand side of Equation (5) are the horizontal and vertical advection. The fourth term is the Coriolis term. The fifth term is the vertical, or turbulent, mixing term. The sixth term is the horizontal mixing term. The last term is the pressure gradient term. Within COAMPS_ATM, the horizontal mixing term (term 6) is set to zero.

Due to the variability between model simulations without data assimilation (i.e., the Gulf Stream in slightly different locations), a point-by-point comparison between the simulations is not informative. Instead, we compare cross-sections centered on the maximum current magnitude along a given longitude that extends $+/-2^\circ$ in latitude. Specifically, for the momentum budget in this example, the Gulf Stream extension maximum current was determined along 71° W for each simulation. The primary 10 m momentum budget terms are shown in Figure 9. The contribution from vertical advection to the total zonal momentum budget was found to be negligible (as expected near the surface), and therefore not shown. As can be seen with the Coriolis term, the atmospheric front is found close to 100 km to the south of the maximum current for the a2o2 simulation and close to 75 km south of the maximum current for the a2o2-cfb simulation. The momentum budget terms are seen to increase in magnitude from approximately 50 km north of the Gulf Stream maximum current to the location of the front south of the maximum current. This is expected due to the corresponding increase in surface winds associated with and behind the front. In each of the simulations, there is largely a balance between the pressure gradient term and the vertical mixing term, in agreement with [8]. However, the zonal advection term has larger contributions with larger wind speeds, i.e., in the frontal region. The relative contribution of the zonal advection term compared to the pressure gradient or vertical mixing terms is also further enhanced in the a2o2-cfb simulation, and is notably greater in magnitude where the current gradients are relatively strong.

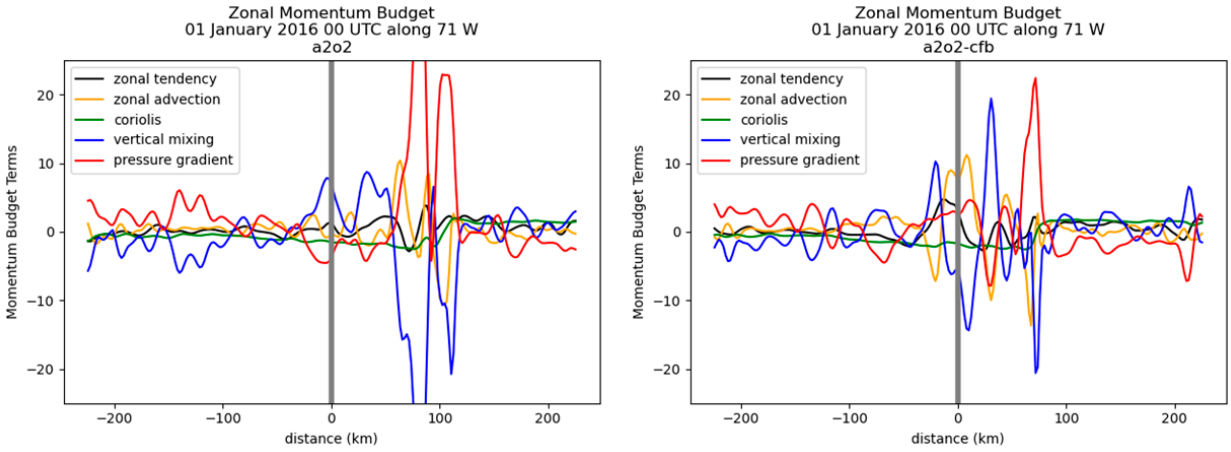

Figure 9. Zonal momentum budget at 10 m along 71° W from 1 January 2016 at 00 UTC for the a2o2 (**left**) and the a2o2-cfb (**right**) simulations. The solid gray line indicates the maximum current in the Gulf Stream extension. The viewpoint is from upstream with north to the left and south to the right of the maximum current.

3.1.4. Dependence on Surface Current Gradients

Many previous studies [6,42,43] have demonstrated that the curl of the surface wind stress is linearly correlated with the crosswind component of the SST gradient, particularly over SST fronts. The authors of [8] additionally investigated and found the relationship between the curl of the wind and the cross-wind component of the current gradient (CWCG) to be important when the current feedback is included, particularly with high resolution models. The CWCG, or the gradient of the current perpendicular to the wind vector, is defined as

$$CWCG = \hat{k} \cdot \left(\nabla \vec{U}_{curr} \times \frac{\vec{U}_{10}}{\left| \vec{U}_{10} \right|} \right) \tag{6}$$

where $\vec{U}_{10}$ is the absolute wind from the model. To better understand the physical processes driving the momentum budget terms, we examined surface processes relevant to horizontal advection. We found the CWCG to be a primary contributing factor driving the horizontal advection.

Following the discussion on the zonal momentum budget, Figure 10 shows the hourly zonal advection PDF binned by the CWCG for 5 days (30 December 2015–3 January 2016) for a smaller region over the Gulf Stream extension (70–73° W and 36–39° N). The wind curl PDF binned by the CWCG is also shown for comparison. Regardless of the current feedback, the zonal advection has a negative relationship with the CWCG, while the wind curl has a positive relationship with the CWCG. A negative CWCG corresponds to negative wind curl [8], as well as positive zonal advection. When the current feedback is included, there is a more extreme systematic shift in the PDF peaks, with positive CWCG having a disproportionally stronger impact with negative zonal advection. Additionally, the PDFs have a wider distribution for stronger CWCGs. This shows that more extreme zonal advection and wind curl values are associated with stronger CWCG when the current feedback is included. It should also be noted that the width of the PDFs indicates that other factors also contribute to the zonal advection and wind curl, although there is organization provided by currents. This finding implies that dependence of the drag coefficient on these other factors (e.g., wind speed and boundary layer stability) have non-negligible impacts on the distribution of relative vorticity.

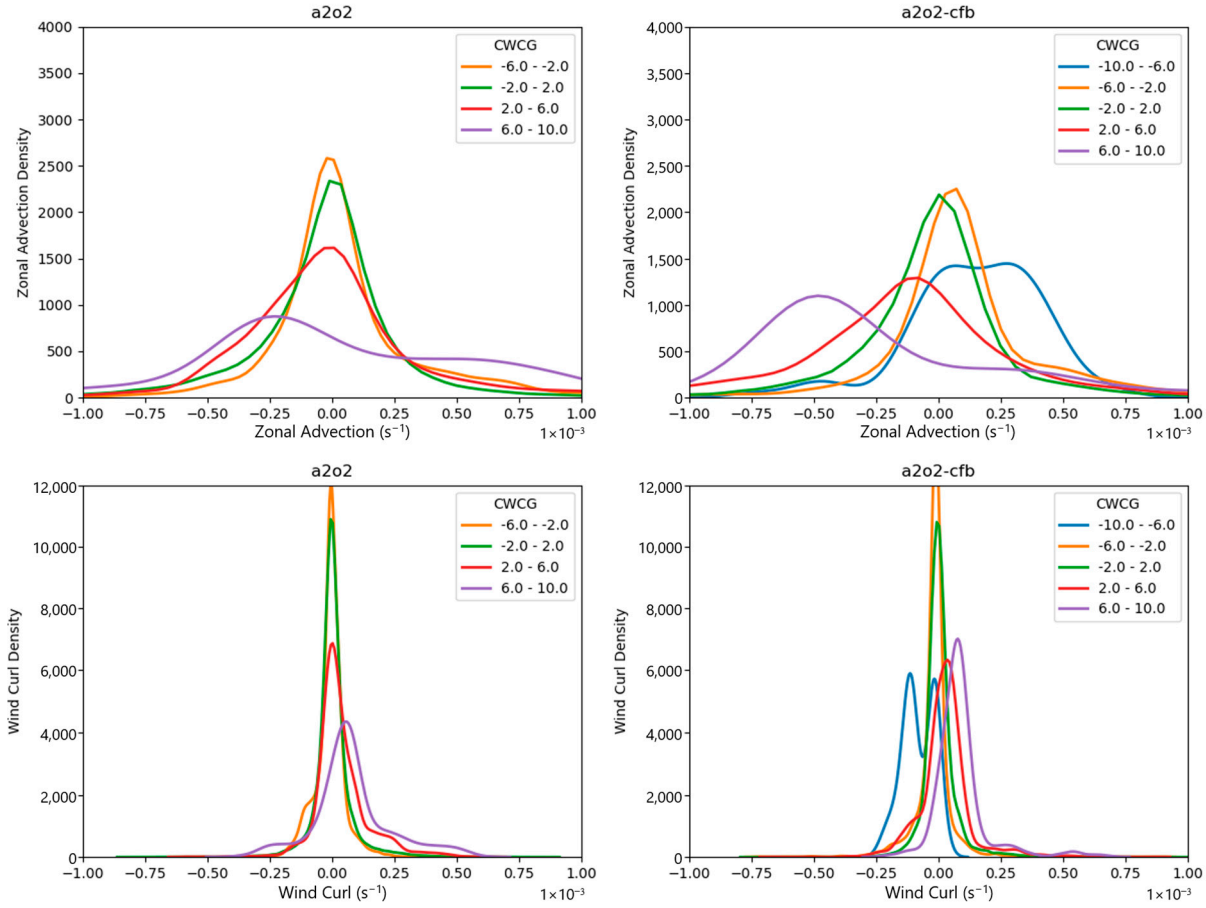

Figure 10. PDFs of the zonal advection (**top**) and wind curl (**bottom**) binned by the cross-wind component of the current gradient (m s^{-1} per 100 km) for 5 days (30 December 2015–3 January 2016) for a smaller region over the Gulf Stream extension (70–73° W and 36–39° N) for the a2o2 (**left**) and the a2o2-cfb (**right**) simulations.

3.2. Secondary Atmospheric Circulation Impacts

Along with the direct changes to atmospheric surface stress and winds when the current feedback is included, there are also secondary impacts (anomalous circulation patterns) within both the atmosphere and the ocean. The secondary circulations in the atmosphere consist of an atmospheric surface divergence, and the vertical integration of the divergence resulting in vertical motion [47–49], as expected from an Ekman model of the atmospheric boundary layer. Here, we explore the current feedback impacts on the secondary circulations over the Gulf Stream extension. Similar to the analysis of the momentum budget, we compare cross-sections along a given longitude that is centered on the maximum current magnitude within the Gulf Stream extension and extends +/−2° in latitude. Specifically, for each simulation, the Gulf Stream maximum current was determined along 70° W every 00:00 UTC analysis time, and then averaged (relative to the location of the maximum current) throughout the winter months (December, January, and February). The winter-season mean vertical cross section of vertical motion (shaded), atmospheric divergence (white contours), and atmospheric vorticity (black contours) is shown in Figure 11. The winter-season mean ocean-relative vorticity for the same cross-section is also included for reference. The maximum current (along 70° W) is denoted at 0 along the *x*-axis with a vertical solid gray line, locations to the north of the maximum current are represented by negative distances, and locations to the south of the maximum current are represented by positive distances. As a reminder, the a2o2 simulation only includes the SST feedback, while the a2o2-cfb simulation includes both the SST feedback

and the current feedback. For this discussion, we focus on the lower atmosphere below 800 mb.

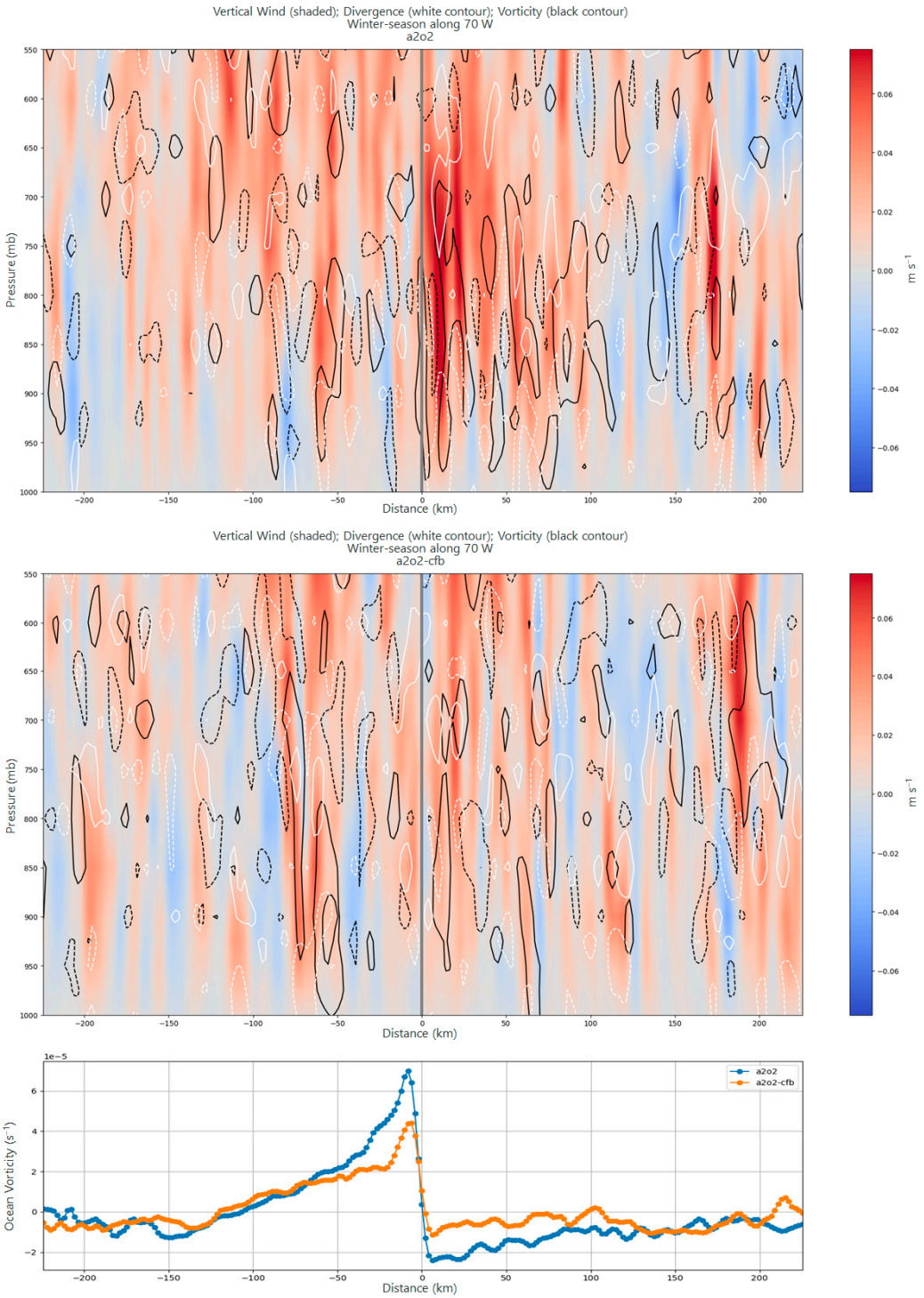

Figure 11. Winter-time seasonal mean of the vertical cross section across the Gulf Stream extension at 70° W for the a2o2 (**top**) and the a2o2-cfb (**middle**) simulations. Vertical motion is shaded, divergence is in white contours, and vorticity is in black contours. Contours are at 3.5×10^{-5} s^{-1} intervals. The solid gray line indicates the maximum current in the Gulf Stream extension. The viewpoint is from upstream with north to the left and south to the right of the maximum current. The (**bottom**) shows the corresponding a2o2 and a2o2-cfb winter-time seasonal mean of the ocean surface vorticity (s^{-1}) across the Gulf Stream extension at 70° W.

To the right (south) of the maximum current in the Gulf Stream extension, there is negative ocean-relative vorticity throughout most of the given range, with slight positive ocean-relative vorticity around 100 km and >200 km from the maximum current. Without the current feedback (a2o2), there is generally low-level convergence (or negative divergence), positive atmospheric vorticity, and upward vertical motion in this section. Including the current feedback (a2o2-cfb) leads to reduced low-level convergence (or increased surface divergence), reduced positive (or increased negative) atmospheric vorticity, and reduced upward (or increased downward) vertical motion.

To the left (north) of the maximum current in the Gulf Stream extension, there is positive ocean-relative vorticity from the maximum current to about 120 km, followed by negative ocean-relative vorticity. Without the current feedback (a2o2), there is overall low-level divergence, negative atmospheric vorticity, and downward vertical motion over the region of positive ocean-relative vorticity. When the current feedback is included (a2o2-cfb), there is increased low-level convergence, increased positive atmospheric vorticity, and enhanced upward vertical motion. Another feature to note from both simulations is enhanced upward vertical motion from the maximum current to approximately 20 km north. This signal is strongly correlated with surface convergence from strong storm systems [42] and frequent atmospheric fronts [36], which exhibit a northward tilt with height.

The atmospheric vorticity and divergence patterns from these simulations are anticipated from the s_w and s_d relationships discussed above. Both the small-scale and large-scale s_w are positive, with enhanced slopes when the current feedback is included. Therefore, when the current feedback is included, there will be enhanced negative wind curl (vorticity) to the right of the maximum current over the negative ocean-relative vorticity and enhanced positive wind curl (vorticity) to the left of the maximum current over the positive ocean-relative vorticity. The small-scale s_d are also positive, with enhanced slopes when the current feedback is included. The large-scale s_d depend on the ocean sign of relative vorticity values, but are always associated with low-level convergence. To the right of the maximum current over negative ocean-relative vorticity, the small-scale and large-scale s_d are counteractive, while to the left of the maximum current over positive ocean-relative vorticity, the small-scale and large-scale s_d are complimentary. Therefore, when the current feedback is included there will be enhanced low-level divergence to the right of the maximum current over the negative ocean-relative vorticity and enhanced low-level convergence to the left of the maximum current over the positive ocean-relative vorticity. It should be noted that these are enhancements to the low-level divergence patterns determined by the SST feedback patterns. In both simulations, areas of low-level divergence are associated with downward vertical motion and areas of low-level convergence are associated with upward vertical motion in the atmospheric boundary layer.

4. Discussion

The physical processes involved in the current feedback identified by [10,12] are further investigated in this study. The primary circulations are discussed in Section 3 and the secondary circulations are discussed in Section 4. As discussed above, when the current feedback is included the primary and secondary circulations cause different feedbacks on either side of the Gulf Stream extension. Both small-scale (<30 km) and large-scale (>30 km) primary and secondary ocean–atmosphere circulations induced by the current gradients, specifically over the Gulf Stream extension, are depicted in Figure 12. The Gulf Stream extension is shown with a green arrow in the middle of the diagram. South is to the right of the Gulf Stream extension and right in the diagram, while North is to the left of the Gulf Stream extension and left in the diagram.

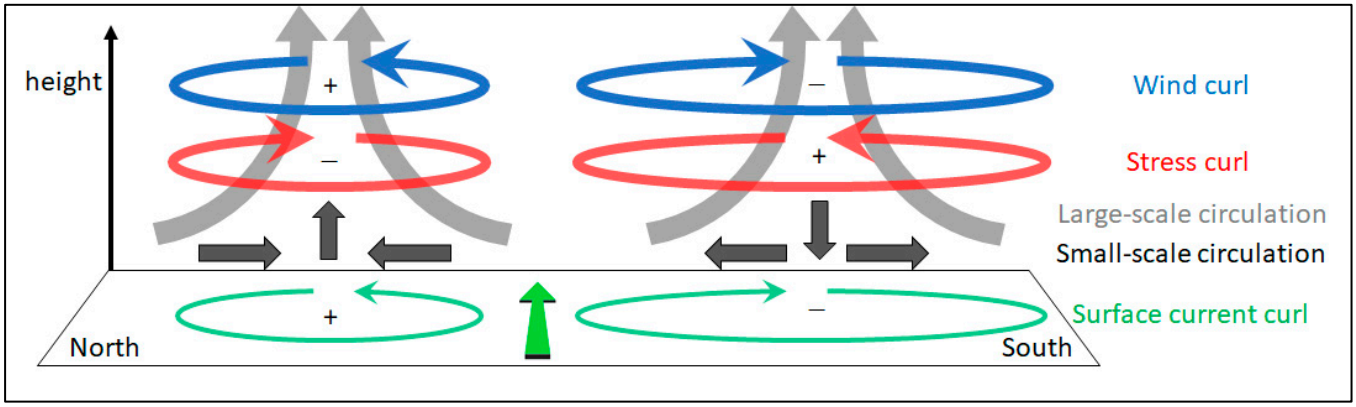

Figure 12. Conceptual diagram of the current feedback impacts over the Gulf Stream extension, with currents and winds moving in the same direction (green arrow). The primary circulations are represented by arrow rings: blue arrow rings indicate wind curl, red arrow rings indicate wind stress curl, and green arrow rings indicate ocean surface vorticity. Secondary circulations (vertical motion and divergence) are represented by grey arrows (large-scale) and black arrows (small-scale). The secondary circulations are in the vertical plane perpendicular to the current.

The primary horizontal circulations shown in this diagram have been identified previously in current feedback modeling studies [8,10,14,33]. The ocean primary horizontal circulation is related to the current-induced ocean-surface-relative vorticity (green arrow rings). The atmospheric primary horizontal circulation anomalies due to currents are related to the curl of the surface stress (red arrow rings) and the curl of the absolute winds (blue arrow rings), which is equal to the curl of the surface currents plus the curl of the surface-relative winds, and is strongly influenced by stress. While the presence of the atmospheric circulations is determined by the inclusion of the current feedback (i.e., allowing the ocean to modify the atmosphere) as well as the thermal feedback, the ocean circulations will exist regardless of feedback, although they can be influenced by changes in the atmosphere [50]. The large-scale and small-scale primary impacts are found to be complimentary to each other.

The secondary circulations are modifications to the primary circulations via feedbacks and are found in the vertical plane perpendicular to the currents. The small-scale secondary atmospheric circulations are depicted with dark grey arrows, while the large-scale secondary circulations are depicted with light grey curved arrows. These circulations consist of the vertical motions and surface divergence associated with the primary circulations, and include the response higher in the atmosphere. The large-scale and small-scale secondary impacts are found to oppose each other over regions of negative ocean-relative vorticity and support each other over regions of positive ocean-relative vorticity. As a reminder, the secondary circulations depicted here are due to the inclusion of the current feedback and do not depict the thermal feedback impacts.

The current feedback impacts on the secondary atmospheric circulations also have further implications. For example, changes in the atmospheric vertical circulation will impact the heat budget in the atmospheric planetary boundary layer (PBL) and the ocean mixed layer (akin to [8]); precipitation depending on the sign of the vertical velocity; and the relative humidity, which could also impact modeled storm intensity. If current gradients are as ubiquitous as suggested by recent global coupled ocean–atmosphere simulations, comprised of the Goddard Earth Observing System (GEOS) atmospheric model coupled to the Massachusetts Institute of Technology general circulation ocean model (MITgcm) [36,51], then changes to atmospheric vertical motion will also change the stratification in the PBL. The change in vertical velocities near the top of the PBL will change the momentum flux throughout the entire PBL, and hence change the horizontal winds near the top of the PBL (in both the PBL and the free atmosphere). This suggests that atmospheric advection of heat and moisture would be slightly modified, which would

impact rainfall on land when that rainfall is related to onshore flow, as is typical for many coastal regions that experience monsoon rains. These impacts suggest that changes to the heat and water cycle could be physically important, not only for weather time-scales, but also for climate time-scales. Studying such impacts requires a high-resolution coupled model, likely run with higher resolution than [51], which produced a data volume from a 14-month simulation that is currently prohibitive to share.

While this study demonstrates the influence current feedback has at the surface as well as throughout the atmospheric boundary layer with the secondary circulation, there are many potential avenues related to the current feedback that have yet to be discussed or studied. While these are not explored in detail here, they are worth highlighting and should be included in future research efforts. First, the region and season for this study was selected due to the increase in submesoscale activity during winter months; however, current feedback impacts due to submesoscale processes and features in other regions and seasons should also be explored. Also, the vertical extent of the secondary circulations is not confined to the surface, but rather extends throughout the atmospheric vertical column (within the troposphere). This implies the current feedback would impact the height of the boundary layer, as well as the exchange between the boundary layer and free atmosphere. Additionally, the secondary circulation impacts are not confined to only the strong current region (i.e., the Gulf Stream extension), but extend to weaker current regions, both north and south of the Gulf Stream extension. The widespread current feedback changes to vertical velocity and surface divergence will also result in changes in cloud formation and precipitation patterns, which will have further impacts on both weather and climate. It is also noted that some changes might enhance storm intensity, while some changes might reduce storm intensity. Thus, a future with stronger or weaker currents could impact the climatology of marine storms. Finally, it should be noted that the selection of model surface flux parameterizations could have a significant impact on the modelling results. Here, we selected the COARE surface flux parameterization, which has been extensively validated with wind speed and boundary layer stability dependent means of in situ observations and is consistent with many previous modelling studies. However, other factors influenced by currents, such as sea state, could play important roles in modifying stress and the ocean/atmosphere coupling examined herein. It is noted, that the stronger response to curl found by [8] using the Taylor and Yelland parameterization [52] would suggest that our impacts will be an underestimation. The dependence of stress on sea state is highly controversial, with substantially different dependencies [15,16], suggesting that a future study should examine the impacts of various sea state dependencies. Careful examination of the relationships presented here—particularly those between ocean-relative vorticity, surface stress curl, and surface wind curl—should be performed using three-way coupled atmosphere–ocean–wave models to assess which model characteristics are sufficiently different to be distinguished with observations.

5. Conclusions

This study uses high-resolution two-way coupled atmosphere–ocean models over the Gulf Stream region to examine the atmospheric dynamic response (both at the surface and throughout the atmospheric boundary layer) of coupling currents to the atmospheric wind stress over a winter season. The direct impact of the current feedback is a modification to the surface stress. When the surface currents and winds are moving in roughly the same direction (typically within the Gulf Stream extension), the current feedback reduces the wind stress and enhances the wind magnitude by modifying the vector wind component parallel the currents. Conversely, when the surface currents and winds are moving in the opposite direction (typically in the northward branch of the Gulf Stream), the current feedback increases the wind stress and reduces the wind magnitude. During typical winter-time conditions (winds and currents flowing in a similar direction), we found the current feedback causes a mean reduction in the wind stress by changing the vertical wind shear

over the Gulf Stream region, and a mean increase to absolute winds by changing their frame of reference and by changing the wind stress.

In addition to the direct surface wind and stress responses to the current feedback, primary horizontal and secondary vertical circulations are also induced. These circulations are summarized with a conceptual diagram (Figure 12) over the Gulf Stream extension. Primary circulations refer to the ocean surface vorticity, the curl of the surface stress, and the wind curl. The secondary circulations are in the vertical plane perpendicular to the current, which consist of the vertical motions and surface divergence closely related to the primary circulation and include the response higher in the atmosphere. The ocean surface vorticity pattern exists regardless of the current feedback. However, the surface stress curl and wind curl patterns only exist when the current feedback is included. These patterns are found to be correlated with the cross-wind component of the current gradient.

To further expand on the present understanding of the current feedback impacts on the atmospheric surface dynamics, we separated the atmospheric surface responses (wind stress, surface wind speed, and surface wind divergence) to the current feedback into small-scale (<30 km) vs. large-scale (>30 km) responses. These responses are commonly referred to as coupling coefficients. When the current feedback is included, the small-scale and large-scale surface stress curl and surface wind curl patterns are shown to be complimentary. The surface stress curl patterns have a negative relationship with the ocean surface vorticity pattern, while the absolute wind curl patterns are shown to have an enhanced positive relationship. During typical winter-time conditions (and presumably other times of year), the small-scale surface wind divergence is found to counter or reduce the effect of the large-scale surface wind divergence over negative ocean vorticity and support or increase the effect of the large-scale surface wind divergence over positive ocean vorticity.

One of the novel findings of this study is that the atmospheric dynamic responses, both at the surface and throughout the atmospheric boundary layer, have a dependency on the relative position of the maximum current within the Gulf Stream extension. Including the current feedback leads to enhanced downward vertical motion in the lower atmosphere with surface divergence to the right of the Gulf Stream extension and enhanced upward vertical motion in the lower atmosphere with surface convergence to the left of the Gulf Stream extension. Because the current feedback impacts both the small-scale and large-scale motions throughout the atmospheric boundary layer, the implication is that it will be important on both weather and climate time-scales.

Author Contributions: Conceptualization, J.M. and M.B.; methodology, J.M. and M.B.; formal analysis, J.M.; investigation, J.M.; resources, J.M.; data curation, J.M.; writing—original draft preparation, J.M.; writing—review and editing, J.M. and M.B.; visualization, J.M.; supervision, M.B.; project administration, J.M. and M.B.; funding acquisition, J.M. and M.B. All authors have read and agreed to the published version of the manuscript.

Funding: J.M. was funded by the U.S. Office of Naval Research as part of the Earth System Prediction Capability project (73-2D27-03-5). M.B. was funded by the Ocean Observing and Monitoring Division, Climate Program Office (FundRef number 100007298), National Oceanic and Atmospheric Administration, U.S. Department of Commerce, through the Northern Gulf of Mexico Institute (NGI grant number 20-NGI3-106), and by NASA PO support for the Ocean Vector Winds Science Team through the Jet Propulsion Laboratory (Contract #1419699).

Institutional Review Board Statement: Not applicable.

Informed Consent Statement: Not applicable.

Data Availability Statement: Due to privacy and ethical concerns, the COAMPS code source cannot be made available; however, the model grid setup and physics are described and provided in Section 2. The atmospheric observations used for data assimilation are available via the Fleet Numerical Meteorology and Oceanography Center (FNMOC) Global Ocean Data Assimilation Experiment (GODAE) server (https://www.usgodae.org/pub/outgoing/fnmoc/data/, accessed on 30 August 2022). The HYCOM and NAVGEM fields used for initial and boundary conditions are available via the HYCOM data server (https://www.hycom.org/dataserver, accessed on 30 August 2022).

The coupled model output fields are too large to be retained or publicly archived with available resources. Documentation and methods used to support this study are available from Jackie May (jackie.may@nrlssc.navy.mil) at the Naval Research Laboratory, Stennis Space Center.

Acknowledgments: We would like to thank Tim Campbell and Travis Smith at NRL Stennis Space Center for their help with setting up and running COAMPS. We would also like to thank Larry O'Neill for providing MATLAB code for computing the high-pass Gaussian filter.

Conflicts of Interest: The authors declare no conflict of interest. The funders had no role in the design of the study; in the collection, analyses, or interpretation of data; in the writing of the manuscript; or in the decision to publish the results.

References

1. Chelton, D.B.; Schlax, M.G.; Samelson, R.M. Summertime Coupling between Sea Surface Temperature and Wind Stress in the California Current System. *J. Phys. Oceanogr.* **2007**, *37*, 495–517. [CrossRef]
2. Spall, M.A. Midlatitude Wind Stress–Sea Surface Temperature Coupling in the Vicinity of Oceanic Fronts. *J. Clim.* **2007**, *20*, 3785–3801. [CrossRef]
3. Small, R.J.; Song, Q.; Cornillon, P.; Spall, M.; Minobe, S. Air–Sea Interaction over Ocean Fronts and Eddies. *Dyn. Atmos. Oceans* **2008**, *45*, 274–319. [CrossRef]
4. Parfitt, R.; Czaja, A.; Minobe, S.; Kuwano-Yoshida, A. The Atmospheric Frontal Response to SST Perturbations in the Gulf Stream Region. *Geophys. Res. Lett.* **2016**, *43*, 2299–2306. [CrossRef]
5. Seo, H.; O'Neill, L.W.; Bourassa, M.A.; Czaja, A.; Drushka, K.; Edson, J.B.; Fox-Kemper, B.; Frenger, I.; Gille, S.T.; Kirtman, B.P.; et al. Ocean Mesoscale and Frontal-Scale Ocean–Atmosphere Interactions and Influence on Large-Scale Climate: A Review. *J. Clim.* **2023**, *36*, 1981–2013. [CrossRef]
6. Chelton, D.B.; Schlax, M.G.; Freilich, M.H.; Milliff, R.F. Satellite Measurements Reveal Persistent Small-Scale Features in Ocean Winds. *Science* **2004**, *303*, 978–983. [CrossRef]
7. O'Neill, L.W.; Chelton, D.B.; Esbensen, S.K. The Effects of SST-Induced Surface Wind Speed and Direction Gradients on Midlatitude Surface Vorticity and Divergence. *J. Clim.* **2010**, *23*, 255–281. [CrossRef]
8. Shi, Q.; Bourassa, M.A. Coupling Ocean Currents and Waves with Wind Stress over the Gulf Stream. *Remote Sens.* **2019**, *11*, 1476. [CrossRef]
9. Bye, J.A.T. Chapter 6 Large-Scale Momentum Exchange in the Coupled Atmosphere-Ocean. In *Elsevier Oceanography Series*; Nihoul, J.C.J., Ed.; Coupled Ocean-Atmosphere Models; Elsevier: Amsterdam, The Netherlands, 1985; Volume 40, pp. 51–61.
10. Renault, L.; Molemaker, M.J.; Gula, J.; Masson, S.; McWilliams, J.C. Control and Stabilization of the Gulf Stream by Oceanic Current Interaction with the Atmosphere. *J. Phys. Oceanogr.* **2016**, *46*, 3439–3453. [CrossRef]
11. Gaube, P.; Chelton, D.B.; Samelson, R.M.; Schlax, M.G.; O'Neill, L.W. Satellite Observations of Mesoscale Eddy-Induced Ekman Pumping. *J. Phys. Oceanogr.* **2015**, *45*, 104–132. [CrossRef]
12. Renault, L.; Molemaker, M.J.; McWilliams, J.C.; Shchepetkin, A.F.; Lemarié, F.; Chelton, D.; Illig, S.; Hall, A. Modulation of Wind Work by Oceanic Current Interaction with the Atmosphere. *J. Phys. Oceanogr.* **2016**, *46*, 1685–1704. [CrossRef]
13. Eden, C.; Dietze, H. Effects of Mesoscale Eddy/Wind Interactions on Biological New Production and Eddy Kinetic Energy. *J. Geophys. Res.* **2009**, *114*, C05023. [CrossRef]
14. Seo, H.; Miller, A.J.; Norris, J.R. Eddy–Wind Interaction in the California Current System: Dynamics and Impacts. *J. Phys. Oceanogr.* **2016**, *46*, 439–459. [CrossRef]
15. Marino, M.; Faraci, C.; Musumeci, R.E. Shoaling Waves Interacting with an Orthogonal Current. *J. Mar. Sci. Eng.* **2020**, *8*, 281. [CrossRef]
16. Faraci, C.; Musumeci, R.E.; Marino, M.; Ruggeri, A.; Carlo, L.; Jensen, B.; Foti, E.; Barbaro, G.; Elsaßer, B. Wave- and Current-Dominated Combined Orthogonal Flows over Fixed Rough Beds. *Cont. Shelf Res.* **2021**, *220*, 104403. [CrossRef]
17. Renault, L.; Masson, S.; Arsouze, T.; Madec, G.; McWilliams, J.C. Recipes for How to Force Oceanic Model Dynamics. *J. Adv. Model. Earth Syst.* **2020**, *12*, e2019MS001715. [CrossRef]
18. Brassington, G.B.; Martin, M.J.; Tolman, H.L.; Akella, S.; Balmeseda, M.; Chambers, C.R.S.; Chassignet, E.; Cummings, J.A.; Drillet, Y.; Jansen, P.A.E.M.; et al. Progress and Challenges in Short- to Medium-Range Coupled Prediction. *J. Oper. Oceanogr.* **2015**, *8*, s239–s258. [CrossRef]
19. Hodur, R.M. The Naval Research Laboratory's Coupled Ocean/Atmosphere Mesoscale Prediction System (COAMPS). *Mon. Weather Rev.* **1997**, *125*, 1414–1430. [CrossRef]
20. Mellor, G.L.; Yamada, T. Development of a Turbulence Closure Model for Geophysical Fluid Problems. *Rev. Geophys.* **1982**, *20*, 851–875. [CrossRef]
21. Fu, Q.; Liou, K.N. On the Correlated K-Distribution Method for Radiative Transfer in Nonhomogeneous Atmospheres. *J. Atmos. Sci.* **1992**, *49*, 2139–2156. [CrossRef]
22. Fu, Q.; Liou, K.N. Parameterization of the Radiative Properties of Cirrus Clouds. *J. Atmos. Sci.* **1993**, *50*, 2008–2025. [CrossRef]
23. Kain, J.S.; Fritsch, J.M. A One-Dimensional Entraining/Detraining Plume Model and Its Application in Convective Parameterization. *J. Atmos. Sci.* **1990**, *47*, 2784–2802. [CrossRef]

24. Kain, J.S.; Fritsch, J.M. Convective Parameterization for Mesoscale Models: The Kain-Fritsch Scheme. In *The Representation of Cumulus Convection in Numerical Models*; Emanuel, K.A., Raymond, D.J., Eds.; American Meteorological Society: Boston, MA, USA, 1993; pp. 165–170. ISBN 978-1-935704-13-3.
25. Hogan, T.; Liu, M.; Ridout, J.; Peng, M.; Whitcomb, T.; Ruston, B.; Reynolds, C.; Eckermann, S.; Moskaitis, J.; Baker, N.; et al. The Navy Global Environmental Model. *Oceanography* **2014**, *27*, 116–125. [CrossRef]
26. Martin, P.J. *Description of the Navy Coastal Ocean Model Version 1.0*; Naval Research Laboratory: Stennis Space Center, MS, USA, 2000; p. 45.
27. Holland, W.R.; Chow, J.C.; Bryan, F.O. Application of a Third-Order Upwind Scheme in the NCAR Ocean Model. *J. Clim.* **1998**, *11*, 1487–1493. [CrossRef]
28. Metzger, E.J.; Smedstad, O.M.; Thoppil, P.; Hurlburt, H.; Cummings, J.; Walcraft, A.; Zamudio, L.; Franklin, D.; Posey, P.; Phelps, M.; et al. US Navy Operational Global Ocean and Arctic Ice Prediction Systems. *Oceanography* **2014**, *27*, 32–43. [CrossRef]
29. Hunke, E.; Lipscomb, W. *CICE: The Los Alamos Sea Ice Model Documentation and Software User's Manual Version 4.0 LA-CC-06-012*; T-3 Fluid Dynamics Group, Los Alamos National Laboratory: Los Alamos, NM, USA, 2010; p. 73.
30. Fairall, C.W.; Bradley, E.F.; Godfrey, J.S.; Wick, G.A.; Edson, J.B.; Young, G.S. Cool-Skin and Warm-Layer Effects on Sea Surface Temperature. *J. Geophys. Res. Oceans* **1996**, *101*, 1295–1308. [CrossRef]
31. Fairall, C.W.; Bradley, E.F.; Rogers, D.P.; Edson, J.B.; Young, G.S. Bulk Parameterization of Air-Sea Fluxes for Tropical Ocean-Global Atmosphere Coupled-Ocean Atmosphere Response Experiment. *J. Geophys. Res. Oceans* **1996**, *101*, 3747–3764. [CrossRef]
32. Weber, R.O. Remarks on the Definition and Estimation of Friction Velocity. *Bound.-Layer Meteorol.* **1999**, *93*, 197–209. [CrossRef]
33. Takatama, K.; Schneider, N. The Role of Back Pressure in the Atmospheric Response to Surface Stress Induced by the Kuroshio. *J. Atmos. Sci.* **2017**, *74*, 597–615. [CrossRef]
34. Jensen, T.G.; Shulman, I.; Wijesekera, H.W.; Anderson, S.; Ladner, S. Submesoscale Features and Their Interaction with Fronts and Internal Tides in a High-Resolution Coupled Atmosphere-Ocean-Wave Model of the Bay of Bengal. *Ocean Dyn.* **2018**, *68*, 391–410. [CrossRef]
35. Renault, L.; McWilliams, J.C.; Gula, J. Dampening of Submesoscale Currents by Air-Sea Stress Coupling in the Californian Upwelling System. *Sci. Rep.* **2018**, *8*, 13388. [CrossRef] [PubMed]
36. Strobach, E.; Klein, P.; Molod, A.; Fahad, A.A.; Trayanov, A.; Menemenlis, D.; Torres, H. Local Air-Sea Interactions at Ocean Mesoscale and Submesoscale in a Western Boundary Current. *Geophys. Res. Lett.* **2022**, *49*, e2021GL097003. [CrossRef]
37. Mensa, J.A.; Garraffo, Z.; Griffa, A.; Özgökmen, T.M.; Haza, A.; Veneziani, M. Seasonality of the Submesoscale Dynamics in the Gulf Stream Region. *Ocean Dyn.* **2013**, *63*, 923–941. [CrossRef]
38. Su, Z.; Wang, J.; Klein, P.; Thompson, A.F.; Menemenlis, D. Ocean Submesoscales as a Key Component of the Global Heat Budget. *Nat. Commun.* **2018**, *9*, 775. [CrossRef] [PubMed]
39. Uchida, T.; Le Sommer, J.; Stern, C.; Abernathey, R.P.; Holdgraf, C.; Albert, A.; Brodeau, L.; Chassignet, E.P.; Xu, X.; Gula, J.; et al. Cloud-Based Framework for Inter-Comparing Submesoscale-Permitting Realistic Ocean Models. *Geosci. Model Dev.* **2022**, *15*, 5829–5856. [CrossRef]
40. Su, Z.; Torres, H.; Klein, P.; Thompson, A.F.; Siegelman, L.; Wang, J.; Menemenlis, D.; Hill, C. High-Frequency Submesoscale Motions Enhance the Upward Vertical Heat Transport in the Global Ocean. *J. Geophys. Res. Oceans* **2020**, *125*, e2020JC016544. [CrossRef]
41. Minobe, S.; Kuwano-Yoshida, A.; Komori, N.; Xie, S.-P.; Small, R.J. Influence of the Gulf Stream on the Troposphere. *Nature* **2008**, *452*, 206–209. [CrossRef]
42. O'Neill, L.W.; Haack, T.; Chelton, D.B.; Skyllingstad, E. The Gulf Stream Convergence Zone in the Time-Mean Winds. *J. Atmos. Sci.* **2017**, *74*, 2383–2412. [CrossRef]
43. Renault, L.; Masson, S.; Oerder, V.; Jullien, S.; Colas, F. Disentangling the Mesoscale Ocean-Atmosphere Interactions. *J. Geophys. Res. Oceans* **2019**, *124*, 2164–2178. [CrossRef]
44. O'Neill, L.W. Wind Speed and Stability Effects on Coupling between Surface Wind Stress and SST Observed from Buoys and Satellite. *J. Clim.* **2012**, *25*, 1544–1569. [CrossRef]
45. Delpech, A.; Barkan, R.; Renault, L.; McWilliams, J.; Siyanbola, O.Q.; Buijsman, M.C.; Arbic, B.K. Wind-Current Feedback Is an Energy Sink for Oceanic Internal Waves. *Sci. Rep.* **2023**, *13*, 5915. [CrossRef]
46. Taylor, J.R. *An Introduction to Error Analysis: The Study of Uncertainties in Physical Measurements*, 2nd ed.; University Science Books: Sausalito, CA, USA, 1997; ISBN 0-935702-75-X.
47. Lettau, H.H. Wind and Temperature Profile Prediction for Diabatic Surface Layers Including Strong Inversion Cases. *Bound.-Layer Meteorol.* **1979**, *17*, 443–464. [CrossRef]
48. Monin, A.S. The Atmospheric Boundary Layer. *Annu. Rev. Fluid Mech.* **1970**, *2*, 225–250. [CrossRef]
49. Pedlosky, J. *Geophysical Fluid Dynamics*, 1st ed.; Springer: Berlin/Heidelberg, Germany; New York, NY, USA, 1979; ISBN 978-0-387-90368-2.
50. Renault, L.; McWilliams, J.C.; Masson, S. Satellite Observations of Imprint of Oceanic Current on Wind Stress by Air-Sea Coupling. *Sci. Rep.* **2017**, *7*, 17747. [CrossRef] [PubMed]

51. Torres, H.S.; Klein, P.; Wang, J.; Wineteer, A.; Qiu, B.; Thompson, A.F.; Renault, L.; Rodriguez, E.; Menemenlis, D.; Molod, A.; et al. Wind Work at the Air-Sea Interface: A Modeling Study in Anticipation of Future Space Missions. *Geosci. Model Dev.* **2022**, *15*, 8041–8058. [CrossRef]
52. Taylor, P.K.; Yelland, M.J. The Dependence of Sea Surface Roughness on the Height and Steepness of the Waves. *J. Phys. Oceanogr.* **2001**, *31*, 572–590. [CrossRef]